

Transient vortex events in the initial value problem for turbulence

D. D. Holm, T-Division and CNLS, MS-B284, Los Alamos National Laboratory, Los Alamos, NM 87545, USA

email: dholm@lanl.gov,

Robert Kerr, Department of Mathematics, University of Arizona, Tucson, AZ 85721, USA

email: kerr@math.arizona.edu

(October 18, 2001)

A vorticity surge event that could be a paradigm for a wide class of bursting events in turbulence is studied to examine how the energy cascade is established and how this event could serve as a new test of LES turbulence models. This vorticity surge event is tied to the formation of the energy cascade in a direct numerical simulation by the traditional signatures of a turbulent energy cascade such as spectra approaching $-5/3$ and strongly Beltramiized vortex tubes. A coherent mechanism is suggested by the nearly simultaneous development of a maximum of the peak vorticity $\|\omega\|_\infty$, growth of the dissipation, the appearance of a helically aligned local vortex configuration and strong, transient oscillations in the helicity wavenumber spectrum. This coherence is also examined for two LES models, a traditional purely dissipative eddy viscosity model and a modern method (LANS- α) that respects the nonlinear transport properties of fluids. Both LES models properly represent the spectral energy and energy dissipation associated with this vorticity surge event. However, only the model that preserves nonlinear fluid transport properties reproduces the helical properties, including Beltrami-like vortex tubes.

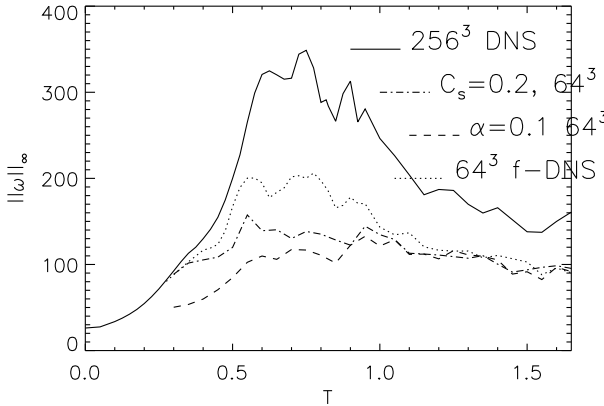


FIG. 1. Comparison of the growth of $\|\omega\|_\infty$ for DNS, 64^3 , $\alpha = 0.05$, and $C_s = 0.2$ Smagorinsky calculations. This figure sets the time scales for our analysis.

Although three-dimensional turbulence is characterized by intermittent events both in space and time, it is often treated as a homogeneous, statistically steady transfer of energy through the spectrum to high wavenumbers accompanied by a $k^{-5/3}$ energy spectrum and a tangled collection of vortex tubes. This statistically-steady description has been useful for the verification of turbulence models through simulations of forced turbulence and smoothly decaying homogeneous,

isotropic turbulence [1–5]. In these studies it is sometimes argued that the initial nonequilibrium transients can be ignored as being non-universal. However, each intermittent burst of turbulence is itself a transient dynamical process in which individual vortex interactions dominate the overall statistical properties. The numerical investigation of the decay of turbulence discussed here continues a long tradition in the numerical modeling of the initial value problems in computational fluid dynamics designed to improve our understanding of individual intermittent events.

Numerically, the question of transient phenomena in turbulence has been considered using a variety of initial conditions [6–9]. In this letter the evolution from smooth, random, initial conditions introduced in [8] to steady turbulent decay is considered from a new viewpoint. Our objective is to apply a coordinated set of diagnostics in both physical and wavenumber space for numerically detecting individual vortex surge events and their subsequent dynamics. These diagnostics show that this initial value problem for turbulence evolves through several complex states in a sequence of transitions. These include:

- formation of vortex sheets that interact, roll up into vortex tubes, then tend to encounter each other transversely,
- development of a peak in the maximum vorticity that is correlated with helicity signatures in both physical and wavenumber space,
- rearrangement of vortex-tubes into transverse configurations that are inherently helical: the velocity \mathbf{u} induced by one vortex tube is aligned with the vorticity $\omega = \text{curl } \mathbf{u}$ of the other tube, as in Beltrami flows – for which the helicity density $\Lambda = \mathbf{u} \cdot \omega$ is maximal.
- formation of the classical decay regime with a $k^{-5/3}$ energy spectrum.

While our analysis also includes traditional diagnostics such as energy decay, our new understanding will arise primarily through: the time evolution of the maximum vorticity in Figure 1; physical space visualizations in Figures 2 and 4; helicity probability distributions in Figure 3; and the accompanying helicity spectrum in Figure 5. Central to our new understanding is the following observation: although this initial condition is not a Beltrami flow, spatial regions do develop during its evolution where the helical alignment measured by $\cos \theta = \Lambda / (u \omega)$ of either sign is locally near unity in magnitude. Evidence is

given that the ensuing dynamics is influenced by helicity. The time scale for this investigation is set by a surge in the growth of the maximum vorticity at $t = 0.5$ in Figure 1. The importance of helicity is demonstrated by the configuration at $t = 0.5$ in Figure 2, by which time the interaction of the initial vortex sheets in the weakly dissipative regime has resulted in nearly orthogonal vortex structures. This is an inherently helical configuration that has arisen from the non-Beltrami initial conditions of [8] simultaneously with the vorticity surge event.

The helical nature of the configuration is shown both by the concentrations of helicity density Λ near the vortex structures in Figure 2 and by a skewed, transient distribution of the cosine of the helicity angle at $t = 0.5$ in Figure 3. The probability density function for $\cos \theta$ at $t = 0.7$ shows that helicity distributions that are initially very small and uniform can eventually develop peaks concentrated at $\cos \theta = \pm 1$ as reported in other turbulent flows [10,11], which Figure 4 shows is associated with the formation of nearly Beltrami vortex tubes. Accompanying this helicity signature in physical space, the helicity spectrum at low wavenumbers in Figure 5 develops a strong signature of alternating sign between wavenumber bands.

$\omega > 0.55\omega_p$, ω lines, $t=0.5$
blue:H<-300, green:H>300

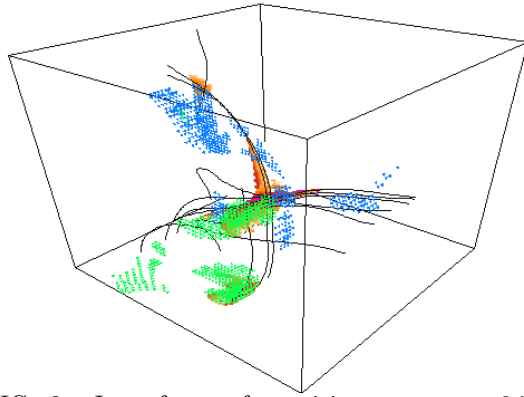


FIG. 2. Isosurfaces of vorticity at $t = 0.5$ where $\omega \geq 0.55\|\omega\|_\infty$ in red/earth colors with sample vortex lines through these regions. Regions of high positive and negative helicity are indicated by green and blue respectively. The vortex lines meet transversely, which is an inherently helical configuration.

Aims and approaches The first aim of this paper is the characterization already given of the stages of the transient vorticity event obtained by direct numerical simulations (DNS). The second aim is the investigation of how our characterization could serve as a new test of large eddy simulation (LES) models. For the latter, we shall compare the results of two different turbulence LES models to our DNS of the Navier-Stokes equations using a pseudospectral code run with 256^3 modes. These models are:

- a standard numerical turbulence model using Smagorinsky diffusion with $C_s = 0.2$ and run with 64^3 modes, and
- the LANS- α model, a new turbulence model based primarily upon dispersion rather than diffusion [12,5,13], also run with 64^3 modes [20].

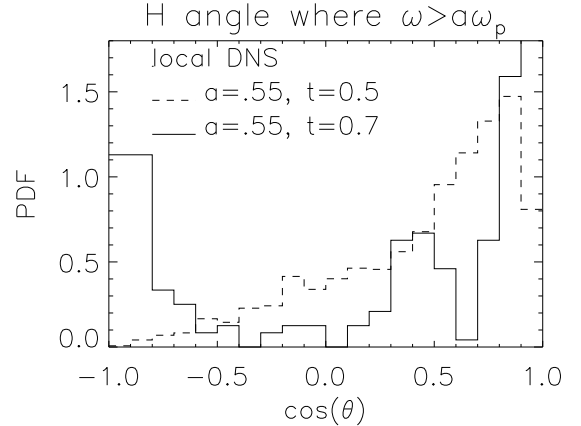


FIG. 3. Probability density functions of the helicity angle $\cos \theta = \vec{u} \cdot \vec{\omega} / (u \omega)$ in physical space at $t = 0.5$, during the surge in the vorticity maximum, and $t = 0.7$ after the initial vortex reconnection. The distribution is taken over those points with vorticity above the shown threshold in the subdomain containing $\|\omega\|_\infty$ at both $t=0.5$ and 0.7. The distribution was initially flat. The asymmetry in the distribution emerges because the transverse vortex configurations that develop are inherently helical.

$\omega > 0.47\omega_p$, ω lines, blue:H<0, green:H>0, DNS $t=0.7$

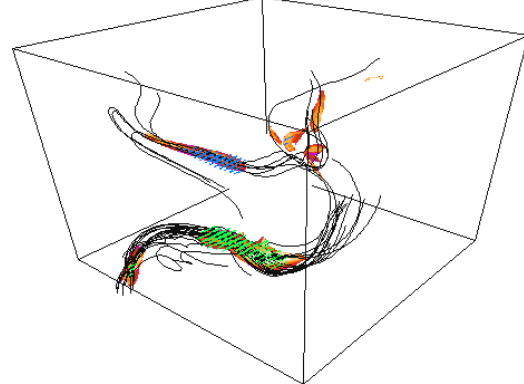


FIG. 4. Isosurfaces of vorticity at $t = 0.7$ where $\omega \geq 0.47\|\omega\|_\infty$ in red/earth colors with sample vortex lines through these regions. Regions of high positive and negative helicity are indicated by green and blue respectively. The visualization volume is centered on the new peak vorticity and rotated with respect to Fig. 2 to emphasize Beltrami nature of the vortex tubes. From another angle, it can be seen that the transverse alignment found in Fig. 2 persists.

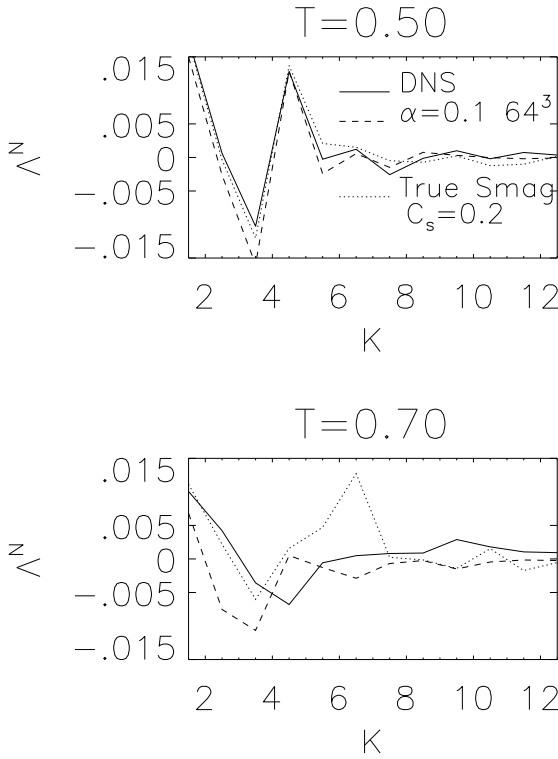


FIG. 5. Comparison of the normalized helicity spectra for the DNS, $\alpha = 0.1$, and Smagorinsky calculations at $t = 0.5$ and $t = 0.7$. The normalization is based upon the energy and enstrophy in the DNS calculations at each time so that comparisons in magnitudes between the different calculations can be made. These strong oscillations first appear at $t \approx 0.45$ when dissipation is still negligible and the vortex structures are beginning to change from sheets to tubes via a roll-up instability induced by interactions between distinct vortex sheets. For the DNS and LANS- α calculations the higher wavenumber oscillations disappear as soon as dissipation is significant, but for the Smagorinsky case they persist longer in a modified form.

The Smagorinsky method is standard, while the LANS- α model is based on a geometrical and dynamical systems approach that concentrates on preserving the nonlinear transport properties of fluid dynamics [14]. The LANS- α equations given in [5,12,13], may be recast equivalently in LES form as

$$\partial_t \mathbf{u} + \mathbf{u} \cdot \nabla \mathbf{u} - \nu \Delta \mathbf{u} - \mathbf{f} + \nabla p + \alpha^2 \operatorname{div} \boldsymbol{\tau} = 0,$$

where pressure p is determined from incompressibility and \mathbf{f} is an external force. The stress tensor $\boldsymbol{\tau}$ in this equation is defined by inverting the Helmholtz operator (with periodic boundary conditions here) in

$$(1 - \alpha^2 \Delta) \boldsymbol{\tau} \equiv \nabla \mathbf{u} \cdot \nabla \mathbf{u} + \nabla \mathbf{u} \cdot \nabla \mathbf{u}^T - \nabla \mathbf{u}^T \cdot \nabla \mathbf{u}.$$

This formulation of the LANS- α model has the same form as the usual Navier-Stokes equations, modulo the additional stress divergence term proportional to α^2 ,

which itself has elements of an LES subgrid-scale turbulence model [15]. Moreover, this subgrid-scale stress tensor formulation admits the same helicity transport properties as the Navier-Stokes equations. Namely, the *helicity density* $\Lambda = \mathbf{u} \cdot \boldsymbol{\omega}$ with $\boldsymbol{\omega} = \operatorname{curl} \mathbf{u}$ obeys, in the absence of forcing,

$$\begin{aligned} \partial_t \Lambda + \operatorname{div}(\mathbf{u} \Lambda + \boldsymbol{\omega} (p - \frac{1}{2} |\mathbf{u}|^2)) - \nu \Delta \Lambda \\ = 2\nu \operatorname{tr}(\nabla \mathbf{u}^T \cdot \nabla \boldsymbol{\omega}) + \alpha^2 \operatorname{div}(\mathbf{u} \times \operatorname{div} \boldsymbol{\tau}) - 2\alpha^2 \boldsymbol{\omega} \cdot \operatorname{div} \boldsymbol{\tau}. \end{aligned}$$

These transport properties determine how helicity decay and generation interacts with subgrid-scale stress models.

During the first stage of evolution, until the onset of the vorticity surge event at time $t = 0.5$, the turbulent calculations we shall compare all have similar behavior. The stage after $t = 0.5$ is when in the DNS the kinetic energy spectrum $E(k)$ begins to move towards the classical $k^{-5/3}$ power-law characteristic of a turbulent energy cascade [8].

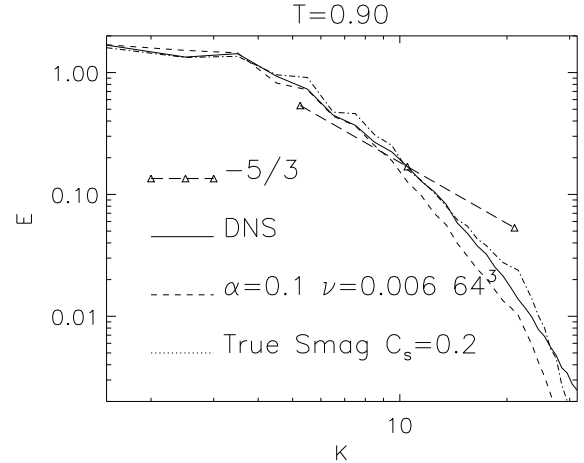


FIG. 6. Comparison of the energy spectra versus the three-dimensional wavenumber by shells for the DNS, 64^3 , $\alpha = 0.1$, and $C_s = 0.2$ Smagorinsky calculations at $t = 0.90$. The energy given for α is $u^2(k)$. The expected $k^{-5/3}$ law has not yet established itself. All the spectra agree at large scales, but the LANS- α spectrum is slightly suppressed at large wavenumbers, which is reflected in a slightly lower total energy at all times.

The energy spectra at $t = 0.9$ in Figure 6 and the energy decay until $t = 1.0$ for all three calculations are similar. Figure 4 at $t = 0.7$ shows that the resulting DNS flow from shortly before this time until the end of the calculation is dominated by isolated vortex tubes in a nearly Beltrami state. These tubes are the source of the strong peak in the helicity distribution at $t = 0.7$ in Figure 3. While this distribution is taken only over the region containing the maximum vorticity, the distribution over the entire domain is similar. The LANS- α calculation is also dominated by vortex tubes and generates local helicity, but the vortex tubes are not as concentrated as

in the DNS renderings in Figure 4. In regions of strong vorticity one sign of the helicity dominates, but over the whole flow LANS- α does not have as strong a signature in the distribution of the helicity angle because it lacks small-scale vortex stretching. The Smagorinsky model, on the other hand, does not show any signature at all in its helicity distribution. Visualizations of Smagorinsky vorticity do show elongated concentrations of vorticity, but helicity is not concentrated in those structures and the structures are not as isolated as in either the DNS or LANS- α calculations.

We conjecture that the difference in the Smagorinsky helicity distributions and vortical structures is associated with the large peak in its helicity spectrum near $k = 6$ in Figure 5. Analysis has shown that the direct source of this helicity peak is the helicity transfer and not the dissipation terms. In all the cases, the helicity transfer spectrum at this intermediate mode begins to grow around $t = 0.55$, perhaps in resonance with other lower wavenumber transfer terms so as to conserve helicity. In the DNS and LANS- α calculations, these intermediate wavenumber transfer terms die out by $t = 0.6$, whereupon higher wavenumber transfer terms transfer helicity from this mode into the dissipation regime. By $t = 0.7$ the positive higher wavenumber peak in the helicity spectrum in the DNS and LANS- α is completely gone. In the Smagorinsky calculation the intermediate modes in the helicity transfer spectrum continue to grow until $t = 0.65$, leading to the stronger intermediate wavenumber helicity peak at $t = 0.7$.

To aid in understanding the origin of the helicity anomalies in the Smagorinsky case, we consider a class of helical shell models [16] based upon the helical triad interactions in Euler [17] similar to the GOY model [18]. In Euler, the strongest triad interactions are between helical wavenumber modes that have oppositely signed helicity. It can be shown with an eddy viscosity, only one sign of helicity is removed in these shell models and that resonant oscillations appear in lower wavenumber shells. This is presently being clarified and could be relevant to the Smagorinsky case where most of the energy dissipation is in the highest, grid-scale, shell of wavenumbers.

Our main conclusions are:

- DNS shows that dynamics involving helicity transport is an integral stage in establishing the turbulent energy cascade from smooth initial conditions.
- The Smagorinsky diffusion method often used in numerical simulations of turbulence does not control transient fluctuations in sign in the helicity spectrum, resulting in anomalous features in the helicity spectrum and a suppression of the expected Beltrami character of small-scale structures.
- LES models that account for fundamental fluid transport properties can accurately model the complex series of transient vortex/helicity events that occur in the initial stages of turbulent dissipation.

Acknowledgements We are grateful to many friends for their enormous help in supplying suggestions, advice and encouragement during the course of this work. In particular, several helpful and timely discussions with S. Y. Chen, G. Eyink, U. Frisch and K. Sreenivasan especially influenced this work.

- [1] R.A. Clark, J.H. Ferziger and W.C. Reynolds, *J. Fluid Mech.* **91**, 1 (1979).
- [2] O. J. McMillan and J. H. Ferziger, *AIAA J.* **17**, 1340 (1979).
- [3] T.S. Lund, in *Annual Research Briefs*, Center for Turbulence Research, NASA Ames - Stanford University, 177 (1991).
- [4] J.R. Chasnov, *Phys. Fluids A* **3**, 188 (1991).
- [5] S. Y. Chen, D. D. Holm, L. G. Margolin and R. Zhang, *Physica D* **133**, 66 (1999).
- [6] M.E. Brachet, D. I. Meiron, S. A. Orszag, B. G. Nickel, R. H. Morf, and U. Frisch, *J. Fluid Mech.* **130**, 411 (1983).
- [7] S. Kida and Y. Murakami, *Phys. Fluid* **30**, 2030 (1987).
- [8] J. R. Herring, R. M. Kerr, *Phys. Fluids A* **5** 2792 (1993).
- [9] R. M. Kerr, *Phys. Fluids A* **5**, 1725 (1993).
- [10] R.B. Pelz, V. Yakhot, S. A. Orszag, L. Shtilman, and E. Levich, *Phys. Rev. Lett.* **54**, 2505 (1985).
- [11] W. Polifke and L. Shtilman, *Phys. Fluids A* **1**, 2025 (1989).
- [12] S. Y. Chen, C. Foias, D. D. Holm, E. J. Olson, E. S. Titi, and S. Wynne, *Phys. Rev. Lett.* **81**, 5338 (1998); *Physica D* **133**, 49 (1999); *Phys. Fluids* **11**, 2343 (1999b).
- [13] C. Foias, D. D. Holm and E. Titi, *Physica D* **152**, 505 (2001); *J. Dyn. and Diff. Eqns.*, to appear (2001).
- [14] D.D. Holm, J.E. Marsden and T.S. Ratiu, *Adv. in Math.* **137**, 1 (1998); *Phys. Rev. Lett.* **80**, 4173 (1998).
- [15] J. A. Domaradzki and D. D. Holm, *ERCOFTAC Bulletin*, **48**, 22 (2001).
- [16] L. Biferale and R. M. Kerr, *Phys. Rev. E* **52**, 6113 (1995).
- [17] F. Waleffe, *Phys. Fluids A* **4**, 350 (1992).
- [18] E.B. Gledzer, *Sov. Phys. Dokl.* **18**, 216 (1973).; K. Ohkitani and M. Yamada, *Prog. Theor. Phys.* **81**, 329 (1989); M. Yamada and K. Ohkitani, *J. Phys. Soc. Jpn.* **56**, 4210 (1987); *Phys. Rev. Lett.* **60**, 983 (1988); *Prog. Theor. Phys.* **79**, 1265 (1988).
- [19] H. K. Moffatt, *J. Fluid Mech.* **35**, 117 (1969).
- [20] LANS- α denotes the Lagrangian-averaged Navier-Stokes α model, in which α is the mean correlation length of fluctuations in Lagrangian fluid trajectories.